CHAPTER 2

Two-Switch High Gain DC-DC Converter

2.1 Introduction

As stated in the previous chapter, a front-end high gain DC-DC converter is required for two-stage AC residential distribution system operated by low voltage DC sources (batteries, fuel and solar cells). This chapter presents a two-switch high gain DC-DC converter (TSHGC) which is derived from single-phase qZSI. Although the circuit arrangement of TSHGC is similar to qZSI, the former gives DC-DC power conversion and can be used as a front-end DC-DC converter for two-stage AC system. The operation and mathematical modeling of TSHGC are discussed and its performance is compared with some reported non-isolated high gain DC-DC converters in terms of a number of elements, voltage gain and device voltage stresses. Simulation and experimental studies are carried out for validation.

2.2 Two-Switch High Gain DC-DC Converter

Fig. 2.1 shows a circuit diagram of TSHGC [105]. It can be observed from Fig. 2.1 that the TSHGC has two switches ($S_1$and S_2), four diodes ($D_1 - D_4$), two capacitors (C_1 and C_2) and two inductors ($L_1$and L_2). The two switches are turned on/off at the same instant. The salient features of TSHGC are as follows.

- It gives high voltage gain using lesser number of elements.
- It has continuous input current due to the presence of an inductor at the input side.
- As it is derived from the qZSI, it can be easily operated for either AC or DC outputs by the switching logic.

As the TSHGC can produce either AC or DC outputs from DC input, DC-DC operation of the TSHGC is only investigated in this chapter. Further, the operation of TSHGC is explained in two intervals; DT_S and $(1 - D)T_s$ in a switching period T_s, where D is the duty ratio and T_s is the switching period.

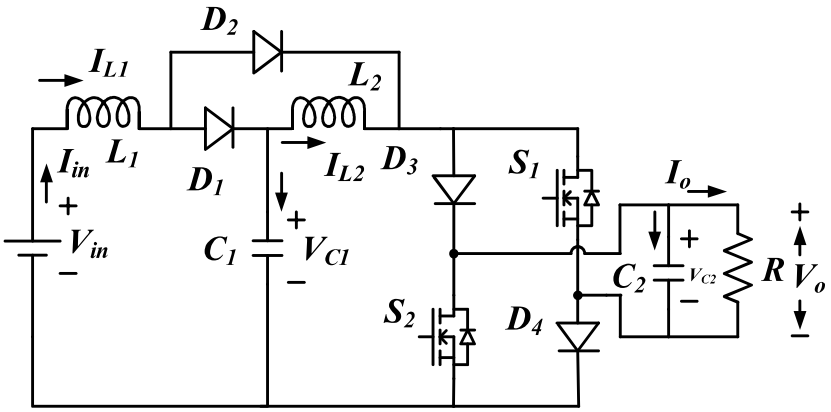

Fig. 2.1. A two-switch high gain DC-DC converter.

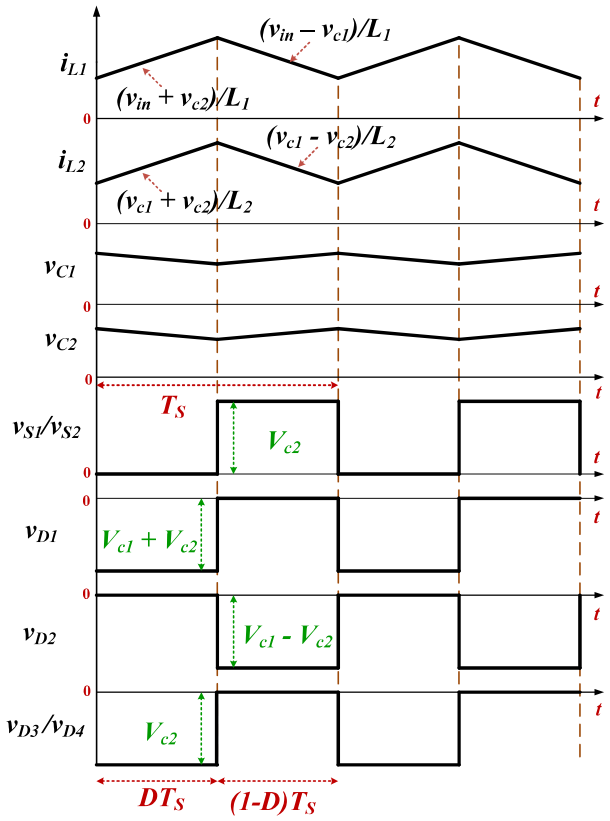

Fig. 2.2. Operating waveforms of TSHGC.

2.2.1 Operation of TSHGC

The operating waveforms of TSHGC are shown in Fig. 2.2 and the equivalent circuits of TSHGC are shown in Fig. 2.3. For DT_S interval, Fig. 2.3(a) shows an equivalent circuit of TSHGC. In this interval, S_1 and S_2 are turned-on along with the forward-biased condition of

D_2. Meanwhile, the diodes (D_1, D_3 and D_4) are reverse-biased. The inductors (L_1 and L_2) are charged and the capacitors ($C_1$and C_2) are discharged during this interval. The obtained Kirchhoff's current law (KCL) and Kirchhoff's voltage law (KVL) equations during the DT_s interval are given in (2.1).

$$\left.\begin{aligned} v_{L1} &= L_1\frac{di_{L1}}{dt} = v_{in} + v_{C2} \\ v_{L2} &= L_2\frac{di_{L2}}{dt} = v_{C1} + v_{C2} \\ i_{C1} &= C_1\frac{dv_{C1}}{dt} = -i_{L2} \\ i_{C2} &= C_2\frac{dv_{C2}}{dt} = -i_{L1} - i_{L2} - i_o \end{aligned}\right\} \tag{2.1}$$

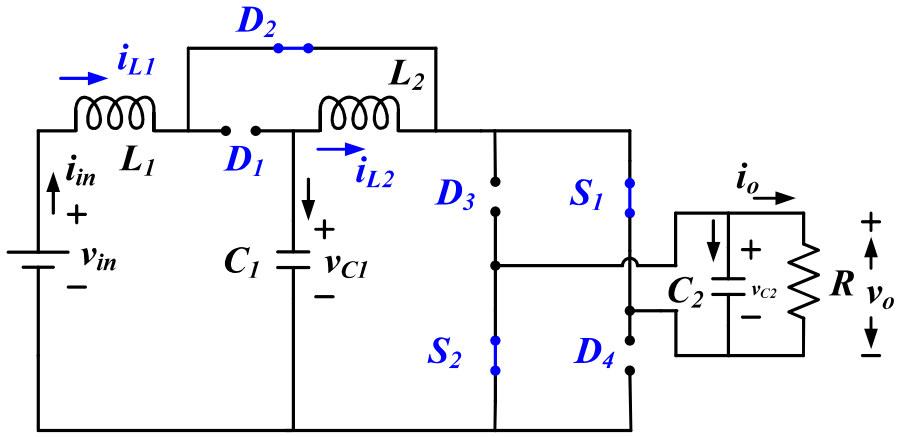

(a)

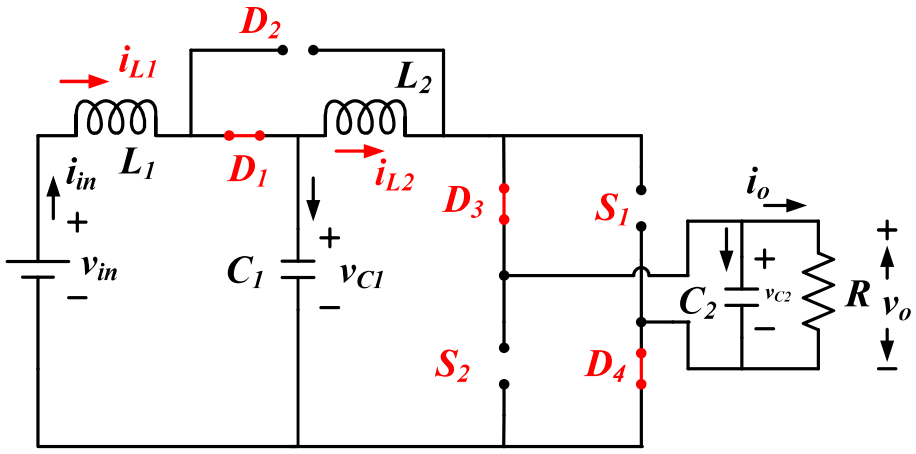

(b)

Fig. 2.3. Equivalent circuits of TSHGC **(a)** during DT_s interval **(b)** during $(1-D)T_s$ interval.

The equivalent circuit of TSHGC during $(1-D)T_s$ interval is shown in Fig. 2.3(b). In this interval, S_1 and S_2 are turned-off. The diode D_2 is reverse biased and diodes (D_1, D_3 and D_4) are forward biased. The stored energy of inductors starts discharging, whereas the capacitors

start charging. The obtained KVL and KCL equations during $(1-D)T_s$ interval are given in (2.2).

$$\left.\begin{aligned} v_{L1} &= L_1 \frac{di_{L1}}{dt} = v_{in} - v_{C1} \\ v_{L2} &= L_2 \frac{di_{L2}}{dt} = v_{C1} - v_{C2} \\ i_{C1} &= C_1 \frac{dv_{C1}}{dt} = i_{L1} - i_{L2} \\ i_{C2} &= C_2 \frac{dv_{C2}}{dt} = i_{L2} - i_o \end{aligned}\right\} \tag{2.2}$$

2.2.2 Steady-State Analysis of TSHGC

After applying volt-second balance principle of an inductor to L_1, $\int_0^{DT_s} v_{L1}\,dt + \int_{DT_s}^{(1-D)T_s} v_{L1}\,dt = 0$, the obtained relation is given in (2.3).

$$V_{in} + DV_{C2} = V_{C1}(1-D) \tag{2.3}$$

Similarly, by applying volt-second balance principle to L_2, the obtained relation is given in (2.4)

$$V_{C1} = V_{C2}(1-2D) \tag{2.4}$$

From (2.3) and (2.4), the steady-state voltage across C_1 is derived and is given in (2.5).

$$V_{C1} = \frac{1-2D}{1-4D+2D^2} V_{in} \tag{2.5}$$

From (2.4) and (2.5), the obtained steady-state voltage across C_2 is given in (2.6).

$$V_{C2} = \frac{1}{1-4D+2D^2} V_{in} \tag{2.6}$$

It can be observed from Fig. 2.3 that the output voltage (V_o) of TSHGC is same as that of V_{C2}. Hence, the steady-state expression of V_o can be rewritten as given in (2.7).

$$V_o = V_{C2} = \frac{1}{1-4D+2D^2} V_{in} \tag{2.7}$$

The voltage gain (G) of TSHGC is defined as the ratio of output and input voltages and its expression is given in (2.8).

$$G = \frac{V_o}{V_{in}} = \frac{1}{1-4D+2D^2} \tag{2.8}$$

After applying charge-second balance principle of a capacitor to C_1, $\int_0^{DT_s} i_{C1}\,dt + \int_{DT_s}^{(1-D)T_s} i_{C1}\,dt = 0$, the obtained relation is given in (2.9).

$$I_{L2} = (1-D)I_{L1} \tag{2.9}$$

Similarly, by applying charge-second balance principle to C_2, the obtained relation is given in (2.10).

$$I_{L2}(1-2D) - I_{L1}(D) = I_o \tag{2.10}$$

From (2.9) and (2.10), the obtained steady-state average currents through L_1 and L_2 are given in (2.11).

$$\left.\begin{aligned} I_{L1} &= I_{in} \\ I_{L2} &= (1-D)I_{in} \\ I_o &= (1-4D+2D^2)I_{in} \end{aligned}\right\} \tag{2.11}$$

2.2.3 Maximum Current and Voltage Stresses on the Elements of TSHGC

The maximum current and voltage stresses on the elements of TSHGC are determined and are given in Table 2.1. Further, the device current and voltage stresses are normalized (by V_{in} and I_{in}) and are plotted with respect to D as shown in Fig. 2.4. It can be observed from Fig. 2.4(a) that the elements (D_1 and L_2) have higher voltage stresses and D_2 has lower voltage stress among other elements of TSHGC. However, the elements (C_2, D_3, D_4, S_1 and S_2) have equal voltage stresses. It can be noticed from Fig. 2.4(b) that C_2 has higher current stress and the elements (C_1, D_3, D_4 and L_2) have lower current stresses as compared to other elements of TSHGC.

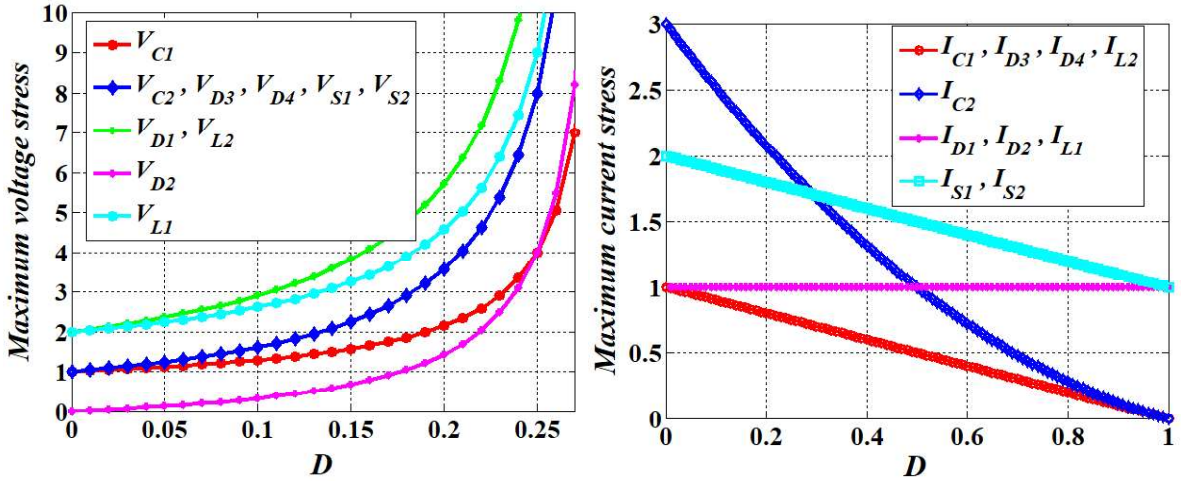

(a) **(b)**

Fig. 2.4. Normalized maximum current and voltage stresses on the elements of TSHGC with respect to D **(a)** maximum device voltage stress **(b)** maximum device current stress.

Table 2.1. Maximum current and voltage stresses on the elements of TSHGC.

	Maximum voltage stress	Maximum current stress
C_1	$\frac{1-2D}{1-4D+2D^2}V_{in}$	$(1-D)I_{in}$
C_2	$\frac{1}{1-4D+2D^2}V_{in}$	$(3-5D+2D^2)I_{in}$
D_1	$\frac{2(1-D)}{1-4D+2D^2}V_{in}$	I_{in}
D_2	$\frac{2D}{1-4D+2D^2}V_{in}$	I_{in}
D_3	$\frac{1}{1-4D+2D^2}V_{in}$	$(1-D)I_{in}$
D_4	$\frac{1}{1-4D+2D^2}V_{in}$	$(1-D)I_{in}$
L_1	$\frac{2-4D+2D^2}{1-4D+2D^2}V_{in}$	I_{in}
L_2	$\frac{2-2D}{1-4D+2D^2}V_{in}$	$(1-D)I_{in}$
S_1	$\frac{1}{1-4D+2D^2}V_{in}$	$(2-D)I_{in}$
S_2	$\frac{1}{1-4D+2D^2}V_{in}$	$(2-D)I_{in}$

2.2.4 Design of Passive Elements of TSHGC

For continuous conduction mode (CCM) operation of TSHGC, expressions for minimum values of passive elements are derived and are given in (2.12).

$$\left.\begin{aligned} L_1 &\geq \frac{V_{in}D(2-4D+2D^2)T_s}{(x_{I_{L1}}\%)I_{in}(1-4D+2D^2)} \\ L_2 &\geq \frac{2V_{in}DT_s}{(x_{I_{L2}}\%)I_{in}(1-4D+2D^2)} \\ C_1 &\geq \frac{I_{in}(1-D)(1-4D+2D^2)DT_s}{(x_{V_{C1}}\%)V_{in}(1-2D)} \\ C_2 &\geq \frac{I_{in}(-3+5D-2D^2)(1-4D+2D^2)DT_s}{(x_{V_{C2}}\%)V_{in}} \end{aligned}\right\} \quad (2.12)$$

where $x_{I_{L1}}\%$ and $x_{I_{L2}}\%$ are percentage ripple in inductor currents, $x_{V_{C1}}\%$ and $x_{V_{C2}}\%$ are percentage ripple in capacitor voltages, D is the duty ratio, T_s is the switching period, V_{in} is the input voltage and I_{in} is the input current.

Further, ripple in inductor currents (ΔI_L) of TSHGC can be calculated from the expression given in (2.13).

$$\Delta I_L = \int_0^{DT_s} \frac{di_L}{dt} dt \tag{2.13}$$

By using (2.13), the obtained ripples in inductor currents of TSHGC are given in (2.14).

$$\left.\begin{aligned} \Delta I_{L1} &= \frac{V_{L1}}{L_1} DT_s \\ \Delta I_{L2} &= \frac{V_{L2}}{L_2} DT_s \end{aligned}\right\} \tag{2.14}$$

where $V_{L1}$and V_{L2} are voltages across L_1 and L_2 during DT_s interval.

Similarly, ripple in capacitor voltages (ΔV_C) of TSHGC can be determined from the expression given in (2.15).

$$\Delta V_C = \int_0^{DT_s} \frac{dV_C}{dt} dt \tag{2.15}$$

By using (2.15), the obtained ripples in capacitor voltages of TSHGC are given in (2.16).

$$\left.\begin{aligned} \Delta V_{C1} &= \frac{I_{C1}}{C_1} DT_s \\ \Delta V_{C2} &= \frac{I_{C2}}{C_2} DT_s \end{aligned}\right\} \tag{2.16}$$

where I_{C1} and I_{C2} are currents through C_1 and C_2 during DT_s interval.

2.3 Comparison Between TSHGC and Some Reported High Gain DC-DC Converters

A comparison among TSHGC and some reported high gain DC-DC converters [34]-[43] is made in terms of number of elements and voltage gain (G) and is given in Table 2.2. The voltage gain of converters is plotted with respect to D as shown in Fig. 2.5. It can be observed from Fig. 2.5 that the converters reported in [38], [40] have higher voltage gain for $D \leq 0.2$ in comparison to converters reported in [39]-[43] and TSHGC. However, converters reported in [39], [40] have higher number of elements and converter reported in [38] has equal number of elements as compared to TSHGC. For $D \geq 0.2$, the TSHGC has higher voltage gain as compared to converters reported in [34]-[43], except the converter reported in [42]. Although converter reported in [42] has higher voltage gain, it has higher number of elements and four bulky inductors as compared to TSHGC, which leads to increase in the volume of the system. Further, voltage stress on the elements (C, $Di.$ and $Sw.$) of TSHGC is calculated and compared with some reported high gain DC-DC converters [34]-[43]. Table 2.3 gives normalized (by V_{in}) total voltage stress on the elements (C, $Di.$ and $Sw.$) of TSHGC and converters reported in [34]-[43]. Fig. 2.6 shows the normalized total voltage stress on the elements of TSHGC and reported converters with respect to D. Fig. 2.6(a) shows normalized total capacitor voltage stress of TSHGC and converters reported in [34]-[40]. It can be

observed from Fig. 2.6(a) that the TSHGC has lower capacitor voltage stress as compared to converters reported in [37]-[40]. Although the converters reported in [34]-[36], [43] have lower capacitor voltage stress in comparison to TSHGC, they have higher number of elements.

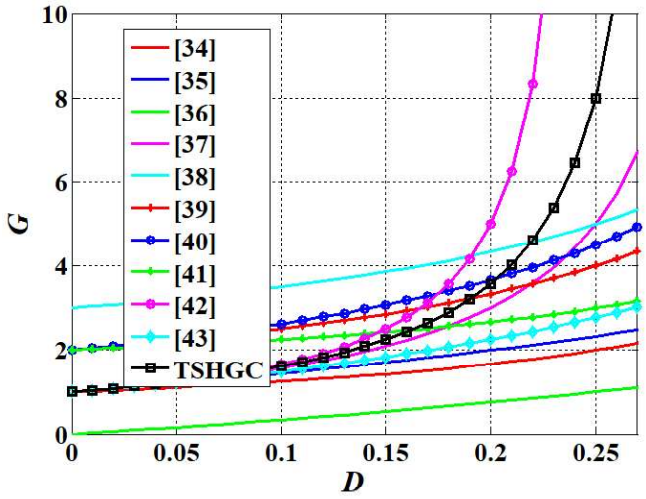

Fig. 2.5. Variation in the G of TSHGC with respect to D in comparison to some reported high gain DC-DC converters.

Table 2.2. Comparison between TSHGC and some reported high gain DC-DC converters.

Converter	C	$Di.$	L	$Sw.$	Total Elements	Gain ($\frac{V_o}{V_{in}}$)
[34]	3	3	3	1	10	$\frac{1}{1-2D}$
[35]	1	7	4	2	14	$\frac{1+3D}{1-D}$
[36]	5	3	3	1	12	$\frac{3D}{1-D}$
[37]	3	8	4	1	16	$\frac{1+D}{1-3D}$
[38]	3	4	1	2	10	$\frac{3-2D}{1-2D}$
[39]	5	4	2	1	12	$\frac{2}{1-2D}$
[40]	7	5	3	1	16	$\frac{2+D}{1-2D}$
[41]	3	2	2	1	8	$\frac{2-2D}{1-2D}$
[42]	7	4	4	1	16	$\frac{1}{1-4D}$
[43]	2	9	4	1	16	$\frac{(1+D)^2}{(1-D)^2}$
Proposed TSHGC	2	4	2	2	10	$\frac{1}{1-4D+2D^2}$

Note: C = Capacitors, $Di.$ = Diodes, L = Inductors, $Sw.$ = Switches

Fig. 2.6(b) shows normalized total diode voltage stress of TSHGC with respect to D in comparison to converters reported in [34]-[43]. It can be noticed from Fig. 2.6(b) that the TSHGC has higher diode voltage stress as compared to converters reported in [34]-[41], [43] and lower diode voltage stress than the converter reported in [42] for $D \geq 0.06$. Fig. 2.6(c) shows normalized total switch voltage stress of TSHGC as compared to converters reported in [34]-[43]. It can also be observed from Fig. 2.6(c) that the TSHGC has higher switch voltage stress as compared to converters reported in [34]-[43], except the converter reported in [37]. Although the TSHGC has higher diode and switch voltage stresses, it has lesser number of elements in comparison to converters reported in [34]-[43].

Table 2.3. Normalized total voltage stress on the devices (C, $Di.$, and $Sw.$) of TSHGC and some reported high gain DC-DC converters.

Converter	$\frac{V_C}{V_{in}}$	$\frac{V_D}{V_{in}}$	$\frac{V_S}{V_{in}}$
[34]	$\frac{2}{1-2D}$	$\frac{2}{1-3D+2D^2}$	$\frac{1}{1-3D+2D^2}$
[35]	$\frac{1+3D}{1-D}$	$\frac{4+4D}{1-D}$	$\frac{2+2D}{1-D}$
[36]	$\frac{9D}{1-D}$	$\frac{3-2D}{1-D}$	$\frac{D}{1-D}$
[37]	$\frac{2+2D}{1-3D}$	$\frac{1+D}{1-3D}$	$\frac{3}{1-3D}$
[38]	$\frac{5-2D}{1-2D}$	$\frac{5}{1-2D}$	$\frac{2}{1-2D}$
[39]	$\frac{4}{1-2D}$	$\frac{4}{1-2D}$	$\frac{1}{1-2D}$
[40]	$\frac{4(1+D)}{1-2D}$	$\frac{5}{1-2D}$	$\frac{1}{1-2D}$
[41]	$\frac{4(1-D)}{1-2D}$	$\frac{2}{1-2D}$	$\frac{1}{1-2D}$
[42]	$\frac{3}{1-4D}$	$\frac{4}{1-4D}$	$\frac{1}{1-4D}$
[43]	$\frac{2(1+D)}{1-2D+D^2}$	$\frac{4+4D+D^2}{1-2D+D^2}$	$\frac{1+2D+D^2}{1-2D+D^2}$
Proposed TSHGC	$\frac{2-2D}{1-4D+2D^2}$	$\frac{4}{1-4D+2D^2}$	$\frac{2}{1-4D+2D^2}$

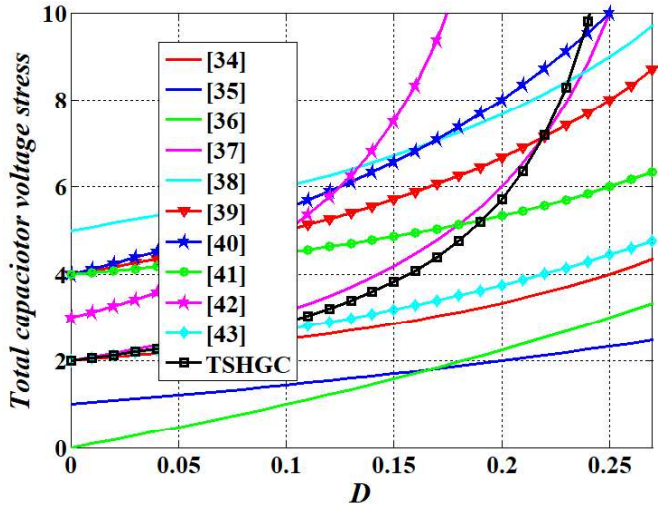

(a)

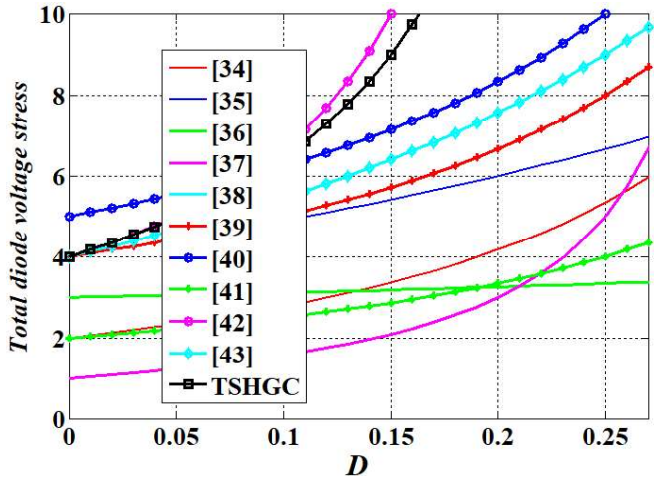

(b)

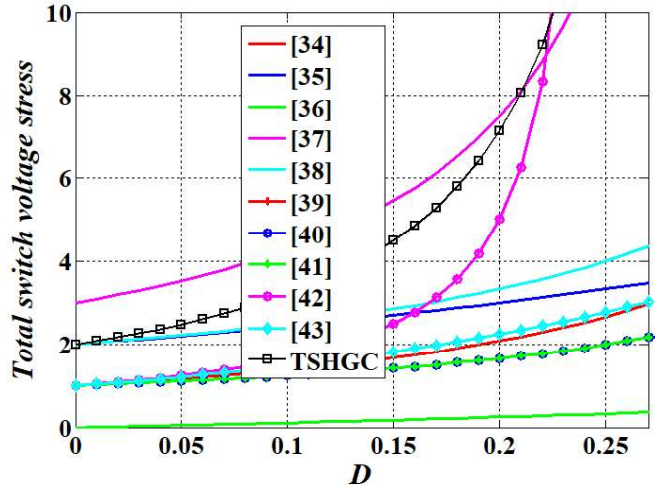

(c)

Fig. 2.6. Normalized total voltage stress on the devices (C, $Di.$, and $Sw.$) of TSHGC and some reported high gain DC-DC converters with respect to D **(a)** normalized total capacitor voltage stress **(b)** normalized total diode voltage stress **(c)** normalized total switch voltage stress.

2.4 Verification of TSHGC

The behaviour of TSHGC is verified through simulation and experimental results. The operating conditions and list of parameters for simulation and experimental studies are given in Table 2.4.

Table 2.4. Operating conditions and list of parameters for the verification of TSHGC.

Parameter	**Value**
Input voltage (V_{in})	24 V
Output power (P_o)	100 W
Duty ratio (D)	0.2
Switching frequency (f_s)	20 kHz
Ripple in inductor currents (Δi_L)	20%
Ripple in capacitor voltages (Δv_c)	3%
Inductor (L_1)	1120 uH
Inductor (L_2)	2240 uH
Capacitor (C_1)	22 uF
Capacitor (C_2)	47 uF

2.4.1 Simulation Results of TSHGC

Fig. 2.7 shows the simulation results of TSHGC for the chosen operating conditions. Moreover, Y-axis in the simulation results consists of voltage/current values having units "V" or "A" and X-axis consists of time values having a unit "s". Fig. 2.7(a) shows output voltage $V_o = 85.6$ V, voltage across capacitors ($C_1$and C_2) $V_{C1} = 51.4$ V and $V_{C2} = 85.6$ V for an input voltage $V_{in} = 24$ V. It can be observed from Fig. 2.7(b) that average currents flowing through inductors (L_1 and L_2) are $I_{L1} = 4.166$ A and $I_{L2} = 3.33$ A along with gate pulse V_{GS} of switches and V_{in}. Moreover, average input current is as same as I_{L1}. Figs. 2.7(c) and 2.7(d) show voltages appearing across power semiconductor devices. It can be observed from Fig. 2.7(c) that voltages experienced by diodes (D_1, D_2 and D_3) are $V_{D1} = -137.1$ V, $V_{D2} = -34.2$ V and $V_{D3} = -85.6$ V along with V_{in}. Fig. 2.7(d) shows voltages across devices (D_4, S_1 and S_2) are $V_{D4} = -85.5$ V, $V_{S1} = 85.3$ V and $V_{S2} = 85.2$ V. It can be concluded from Figs. 2.7(c) and 2.7(d) that D_1 has higher voltage stress and D_2 has lower voltage stress among the power semiconductor devices of TSHGC. Also, devices (D_3, D_4, S_1 and S_2) experience same voltage stress which is equal to V_o of TSHGC.

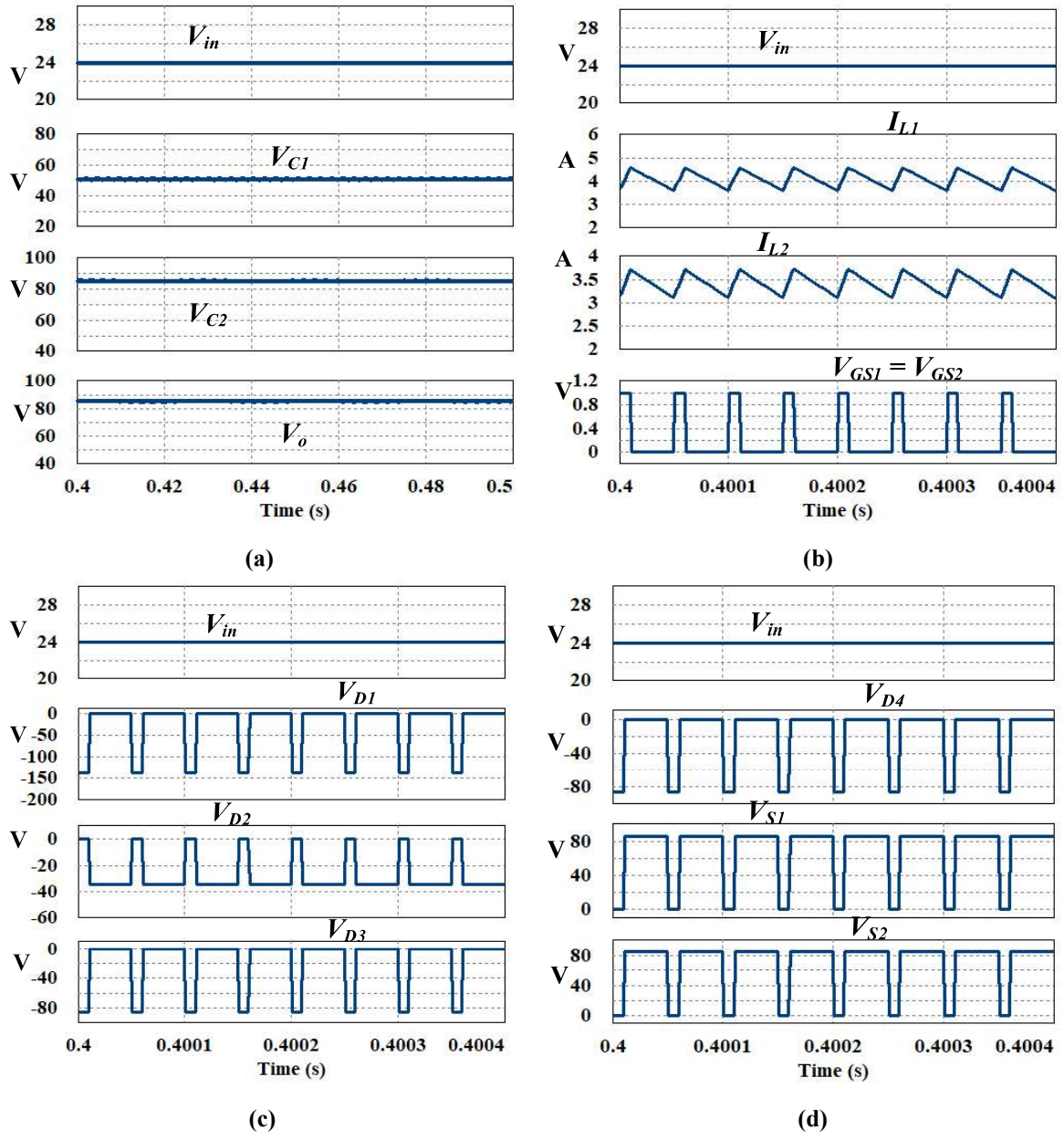

Fig. 2.7. Simulation results of TSHGC **(a)** V_{C1}, V_{C2}, V_o, and V_{in} **(b)** V_{Gs}, I_{L1}, I_{L2}, and V_{in} **(c)** V_{D1}, V_{D2}, V_{D3}, and V_{in} **(d)** V_{D4}, V_{S1}, V_{S2}, and V_{in}. **[Y-axis has voltage/current values, having units "V" or "A"]**

2.4.2 Experimental Results of TSHGC

Fig. 2.8 shows a photograph of the experimental set-up of TSHGC. The experimentation of TSHGC is carried out for same operating conditions as that of the simulation studies and the experimental results are shown in Fig. 2.9. It can be observed from Fig. 2.9(a) that output voltage $V_o = 80.3$ V and voltage across C_1, $V_{C1} = 49.2$ V for an input voltage $V_{in} = 24$ V. Moreover, voltage across C_2 is same as V_o. Fig. 2.9(b) shows average currents flowing through inductors are $I_{L1} = 4.32$ A and $I_{L2} = 3.45$ A along with V_{Gs} and V_{in}. The I_{L1} and I_{L2} have raising slope during on-period of V_{GS} and falling slope during off-period of V_{GS}. Also, average input current of TSHGC is same as I_{L1}. Figs. 2.9(c) and 2.9(d) show voltages appearing across power semiconductor devices of TSHGC. It can be noticed from Fig. 2.9(c) that voltages experienced by diodes (D_1, D_2 and D_3) are $V_{D1} = -132.3$ V, $V_{D2} = -31.4$ V and $V_{D3} = -81.2$ V along with V_{in}. Fig. 2.9(d) shows voltages appearing across devices (D_4, S_1 and S_2) are $V_{D4} = -80.9$ $V_{S1} = 81.2$ V and $V_{S2} = 81.1$ V. It can be concluded from Figs. 2.9(c) and 2.9(d) that D_1 has higher voltage stress which is greater than V_o of TSHGC and D_2 has lower voltage stress among the power semiconductor devices of TSHGC.

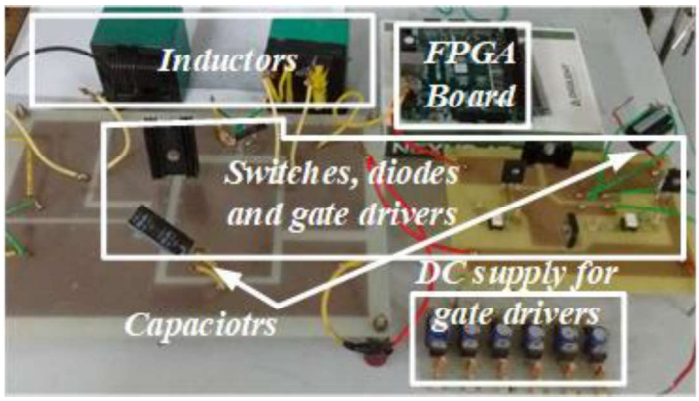

Fig. 2.8. A photograph of the experimental set-up of TSHGC.

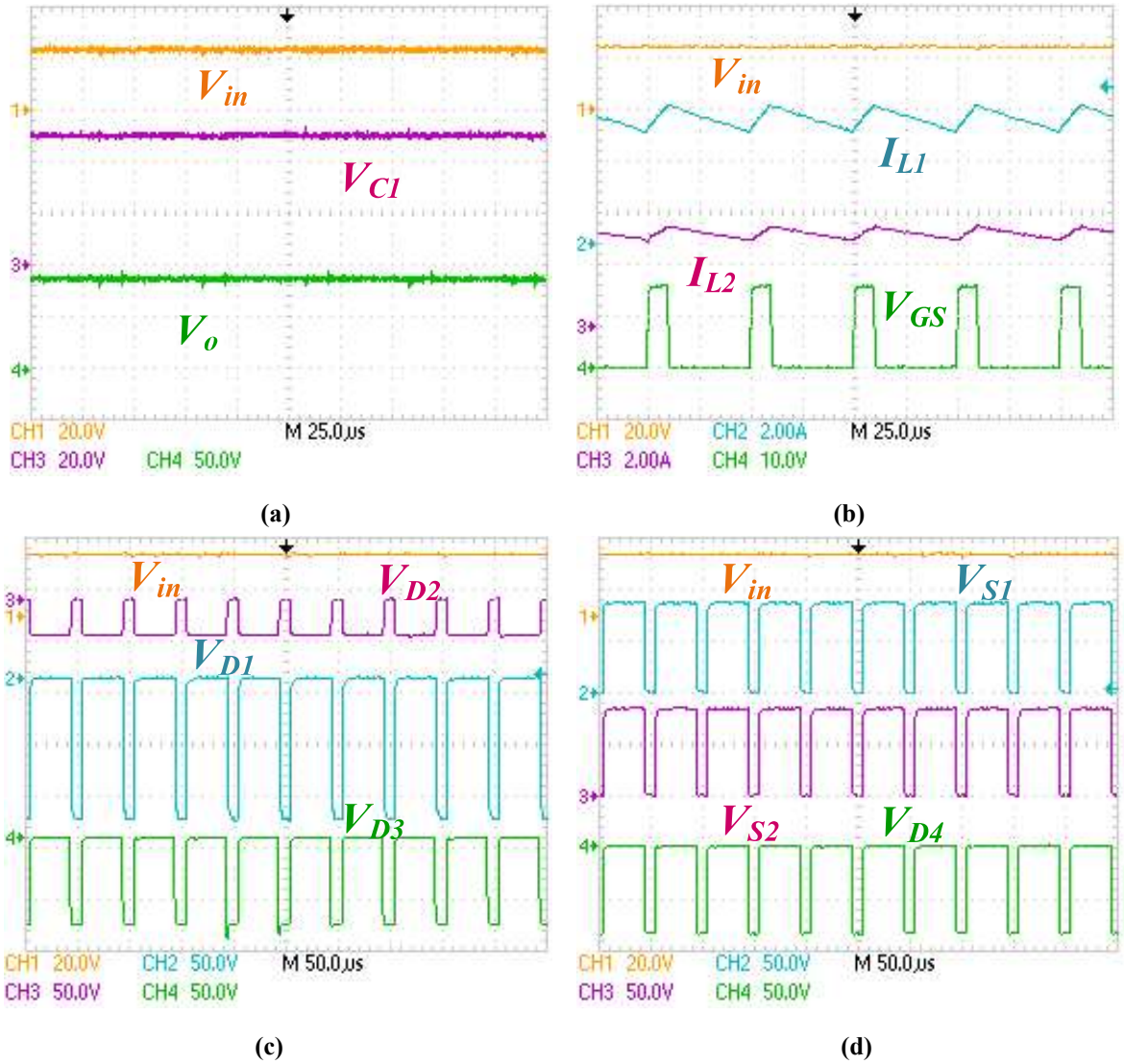

Fig. 2.9. Experimental results of TSHGC **(a)** V_{C1}, V_o, and V_{in} **(b)** V_{GS}, I_{L1}, I_{L2}, and V_{in} **(c)** V_{D1}, V_{D2}, V_{D3}, and V_{in} **(d)** V_{D4}, V_{S1}, V_{S2}, and V_{in}.

2.4.3 Power Loss Calculations and Variation in Efficiency of TSHGC

The power loss calculations include losses due to ESR of capacitors, losses due to DCR of inductors, losses due to conduction and switching states of switches and conduction and reverse recovery (switching) losses in diodes [106]-[112].

(a) Power Losses in Switches of TSHGC

The conduction losses in switches (S_1 and S_2) of TSHGC, P_{S_cond} can be calculated using (2.17).

$$P_{S\_cond} = {I_{S1,rms}}^2 * r_{DS(on),S1} + {I_{S2,rms}}^2 * r_{DS(on),S2} \tag{2.17}$$

The required root mean square (RMS) currents for calculating switch conduction losses can be determined using (2.18).

$$\left.\begin{aligned} I_{S1\_rms} &= \left(\frac{1}{T_s}\int_0^{T_s}(i_{L1}+i_{L2})dt\right)^{\frac{1}{2}} \\ I_{S2\_rms} &= \left(\frac{1}{T_s}\int_0^{T_s}(i_{L1}+i_{L2})dt\right)^{\frac{1}{2}} \end{aligned}\right\} \tag{2.18}$$

where $r_{DS(on),S1}$ and $r_{DS(on),S2}$ are on-state resistances of switches, and those can be known from manufacturer's datasheet of switches.

The switching losses in switches (S_1 and S_2) of TSHGC, P_{S_switc} can be obtained using (2.19).

$$P_{S\_switc} = \left[\frac{1}{2} * I_{S1,avg} * V_{S1} * \left(T_{on,S1} + T_{off,S1}\right) * f_s\right] + \left[\frac{1}{2} * I_{S2,avg} * V_{S2} * \left(T_{on,S2} + T_{off,S2}\right) * f_s\right] \tag{2.19}$$

The required currents and voltages for calculating P_{S_switc} of TSHGC are given in (2.20).

$$\left.\begin{aligned} V_{S1} = V_{S2} &= \frac{1}{1-4D+2D^2}V_{in} \\ I_{S1} = I_{S2} &= D(I_{L_1} + I_{L_2}) \end{aligned}\right\} \tag{2.20}$$

(b) Power Losses in Diodes of TSHGC

The conduction losses in diodes ($D_1 - D_4$) of TSHGC, P_{D_cond} can be obtained using (2.21).

$$P_{D\_cond} = \left[\left(I_{D,avg} * V_{F,D}\right) + \left({I_{D,rms}}^2 * r_{F,D}\right)\right] \tag{2.21}$$

The required average and RMS currents of diodes for calculating P_{D_cond} are given in (2.22) and (2.23), respectively.

$$\left.\begin{aligned} I_{D1,avg} &= (1-D)I_{L1} \\ I_{D2,avg} &= DI_{L1} \\ I_{D3,avg} = I_{D4,avg} &= (1-D)I_{L2} \end{aligned}\right\} \tag{2.22}$$

$$\left.\begin{aligned} I_{D1\_rms} = I_{D2\_rms} &= \left(\frac{1}{T_s}\int_0^{T_s}(i_{L1})dt\right)^{\frac{1}{2}} \\ I_{D3\_rms} = I_{D4\_rms} &= \left(\frac{1}{T_s}\int_0^{T_s}(i_{L2})dt\right)^{\frac{1}{2}} \end{aligned}\right\} \tag{2.23}$$

where $V_{F,D}$ is the forward voltage drop of diodes and $r_{F,D}$ is the forward resistance of diodes, and can be known from manufacturer's datasheet of diodes.

The switching losses in diodes of TSHGC, P_{D_switc} can be determined using (2.24).

$$P_{D\_switc} = \left[\frac{1}{2} * (T_{RR} * I_{RR}) * V_D * f_s\right] \tag{2.24}$$

The required diodes voltages for calculating P_{D_switc} are given in (2.25).

$$\left.\begin{aligned} V_{D1} &= \frac{2(1-D)}{1-4D+2D^2} V_{in} \\ V_{D2} &= \frac{2D}{1-4D+2D^2} V_{in} \\ V_{D3} = V_{D4} &= \frac{1}{1-4D+2D^2} V_{in} \end{aligned}\right\} \tag{2.25}$$

where T_{RR} is the reverse recovery time and I_{RR} is the reverse recovery current of diodes, and can be known from manufacturer's datasheet of diodes.

(c) Power Losses in Capacitors of TSHGC

The power losses in capacitors (C_1 and C_2) of TSHGC, P_C can be determined using (2.26).

$$P_C = \left({I_{C1,rms}}^2 * r_{ESR,C1}\right) + \left({I_{C2,rms}}^2 * r_{ESR,C2}\right) \tag{2.26}$$

The required RMS currents for calculating P_C are given in (2.27).

$$\left.\begin{aligned} I_{C1\_rms} &= \left(\frac{1}{T_s}\int_0^{T_s} i_{C1} dt\right)^{\frac{1}{2}} \\ I_{C2\_rms} &= \left(\frac{1}{T_s}\int_0^{T_s} i_{C2} dt\right)^{\frac{1}{2}} \end{aligned}\right\} \tag{2.27}$$

Further, the i_{C1} and i_{C2} have following relations over the switching period T_S.

$$\left.\begin{aligned} i_{C1} &= -i_{L2} \\ &= i_{L1} - i_{L2} \end{aligned}\right\} \tag{2.28}$$

$$\left.\begin{aligned} i_{C2} &= -i_{L1} - i_{L2} - i_o \\ &= i_{L2} - i_o \end{aligned}\right\} \tag{2.29}$$

where $r_{ESR,C1}$ and $r_{ESR,C2}$ are ESRs of C_1 and C_2 respectively.

(d) Power Losses in Inductors of TSHGC

The power losses in inductors (L_1 and L_2) of TSHGC, P_L can be obtained using (2.30).

$$P_L = \left({I_{L1,rms}}^2 * r_{DCR,L1}\right) + \left({I_{L2,rms}}^2 * r_{DCR,L2}\right) \tag{2.30}$$

The required RMS currents for calculating P_L are given in (2.31).

$$\left.\begin{aligned} I_{L1\_rms} &= \left(\frac{1}{T_s}\int_0^{T_s} i_{L1} dt\right)^{\frac{1}{2}} \\ I_{L2\_rms} &= \left(\frac{1}{T_s}\int_0^{T_s} i_{L2} dt\right)^{\frac{1}{2}} \end{aligned}\right\} \tag{2.31}$$

where $r_{DCR,L1}$ and $r_{DCR,L2}$ are DCRs of L_1 and L_2 respectively.

Based on the above power loss calculations, the power losses are determined by considering non-idealities of elements: (1) $r_{ESR,C1} = 40$ mΩ and $r_{ESR,C2} = 70$ mΩ, (2) $V_{DS(on)} = 1.1$ V and $r_{DS(on)} = 0.15$ Ω, (3) $r_{DCR,L1} = r_{DCR,L2} = 360$ mΩ and (4) $V_{F,D} = 0.8$ V and $r_{F,D} = 0.1$ Ω. The determined power losses in the elements of TSHGC are shown in Fig. 2.10(a) at rated power as a percentage of total power loss. It can be observed from Fig. 2.10(a) that diode power losses are higher than other elements at rated power. Fig. 2.10(b) shows variation in efficiency of TSHGC under different loading conditions. It can be observed from Fig. 2.10(b) that the TSHGC has maximum efficiency as 90.32% at 81 W.

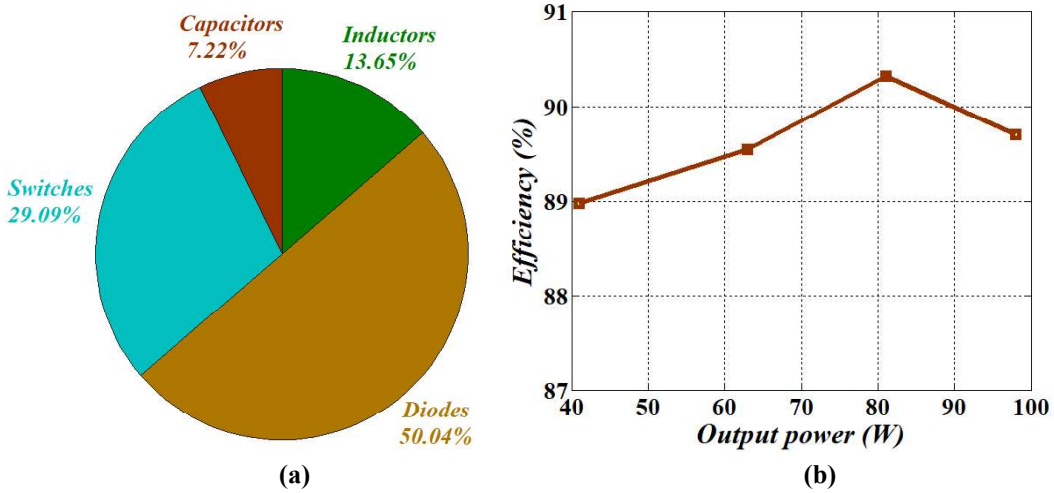

Fig. 2.10. Power loss distribution among the elements and variation in efficiency of TSHGC **(a)** power losses in the elements of TSHGC as a percentage of total power losses **(b)** efficiency variation under different loading conditions.

2.5 Summary

In this chapter, TSHGC has been presented. It gives high voltage gain at a lower value of *D* with reduced elements. It has continuous input current, which is an essential requirement for low voltage sources (batteries, solar and fuel cells) to enhance their life span. Detailed mathematical modeling of TSHGC is given in this chapter to study its operation. A comparison among TSHGC and some reported high gain DC-DC converters is being carried in terms of voltage gain and the number of elements used. It can be concluded from the comparison that some DC-DC converters have high voltage gain in comparison to TSHGC; however they have higher number of elements which results in increased volume and reduced power density of the converters. The performance of TSHGC is verified through simulation and experimental results. Moreover, power losses in the elements of TSHGC are calculated at

rated power and efficiencies at different loading conditions are measured to show its effectiveness. The proposed TSHGC is well suited for two-stage AC system as a front-end DC-DC converter.

Although the TSHGC has continuous input current, it requires a high value of inductance for achieving low ripple in input current. Also, it has a floating output ground with respect to the input ground. To take care of these issues, chapter 3 presents a high gain interleaved boost converter (HGIBC). The HGIBC has two parallelly connected inductors at input side to achieve continuous input current with reduced ripple. Also, input and output voltage ground terminals of HGIBC have a common ground.